NANO LETTERS

2004
Vol. 4, No. 4
709−712

Carbon Nanotube Based Bearing for Rotational Motions

Bertrand Bourlon,[†] D. Christian Glattli,[†,§] Csilla Miko,[‡] Laszlo Forró,[‡] and Adrian Bachtold*,[†]

Laboratoire de Physique de la Matière Condensée de l'Ecole Normale Supérieure, 24 rue Lhomond, 75231 Paris 05, France, and EPFL, CH-1015, Lausanne, Switzerland

Received December 19, 2003; Revised Manuscript Received February 11, 2004

ABSTRACT

We describe the fabrication of a nanoelectromechanical system consisting of a plate rotating around a multiwalled nanotube bearing. The nanotube has been engineered so that the sliding happens between different shells. The motion is possible thanks to the low static intershell friction, which we have estimated to be ∼0.85 MPa.

Microfabricated motors have been among the most studied microelectromechanical systems in the 80s and 90s.[1−3] These motors made of Si are typically several tens of microns in size. Many efforts have been invested in improving performance characteristics such as the rotational speed. It has been shown that the characteristics are mostly limited by the fabrication process through the low reproduction accuracy of the design geometry.[3] For example, microfabrication techniques cannot create surfaces that are regular enough at the contact between the rotor and the bearing. These irregularities are important sources of energy loss and they reduce considerably the rotational speed.

Fennimore et al. have recently reported the fabrication of a motor with much smaller dimensions[4] where the bearing is ∼10 nm in diameter. The key component of this nanoelectromechanical system (NEMS)[5,6] is a multiwalled carbon nanotube (MWNT) which is the source of rotational degree of freedom for the rotor. Indeed, MWNTs consist of several nested cylindrical shells with atomically smooth surfaces enabling easy intershell sliding, as it has been recently measured[7,8] and theoretically studied.[9−14] The rotor plate is made to rotate around the MWNT with the motion that is activated electrostatically through three stator electrodes. In the sample fabrication, the rotor is first attached on the pristine MWNT fixed to two anchor pads. The rotational freedom is obtained by mechanically fatiguing and shearing the MWNT by successive application of large voltages between the rotor and the stators. The rotor is then free to move, but the modifications brought to the MWNT are not controlled well enough to unambiguously determine how the shells move during the actuation of the rotor. Probably, a short section of the outer shell has been removed in the region between the plate and the anchors, enabling part of the outer shell to slide around the inner ones. This rotating part, which is attached to the rotor, is fixed in the direction of the tube axis by the rest of the outer shell.

We have fabricated an electromechanical rotational actuator with a new layout that defines better the motion of the shells. Here, the rotating plate is attached to an inner MWNT shell that turns inside outer shells fixed to two anchor pads (Figure 1A). The plate cannot slide in the direction of the tube axis because it is held by the shell caps. The fabrication of such a device has been made possible with the recently developed electrical-breakdown technique,[15−17] which engineers the MWNT by opening access to the inner shells. During the rotational motion, the plate is observed to be blocked at some specific angles that are associated with some disorder situated along the shells. Our well-defined NEMS enables to estimate the corresponding static friction against rotational sliding, which is found to be ∼0.85 MPa. This is comparable in magnitude to values obtained for intershell friction in the tube axis,[7,8] which has been recently measured in challenging experiments where the MWNTs have been telescoped with one end attached to a manipulator arm[7] or an atomic force microscope probe[8] inside electron microscopes. Importantly, even if disorder is present and enhances friction in our samples, it is weak enough to not completely stick the rotor, which is remarkable given the detrimental effect of unclean surfaces in NEMS actuation. Our results show that our fabrication process is suitable for the realization of electromechanical rotational actuators.

The NEMSs are fabricated through a four-step process. The MWNTs synthesized by arc-discharge evaporation are

* Corresponding author. E-mail: bachtold@lpa.ens.fr.
† Ecole Normale Supérieure de Paris.
‡ EPFL Lausanne.
§ Also at: SPEC, CEA Saclay, F-91191 Gif-sur-Yvette, France.

10.1021/nl035217g CCC: $27.50
Published on Web 03/09/2004

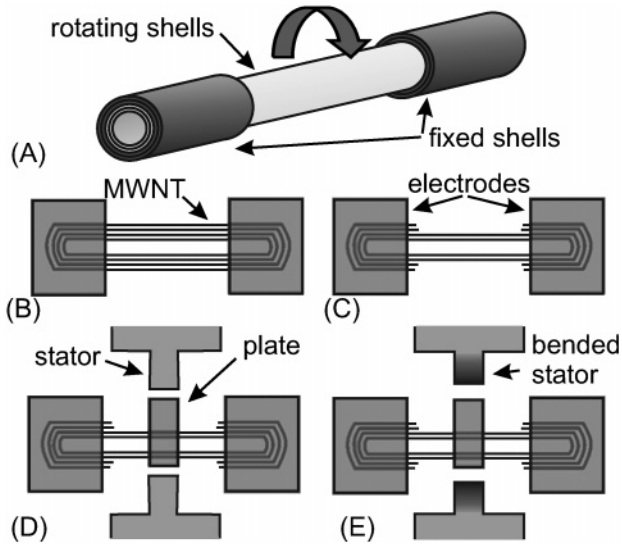

Figure 1. (A) Inner shells turn inside fixed outer shells. (B) The MWNT is contacted to two conducting anchor pads made of 10 nm Cr and 60 nm Au and separated by around 1 μm. (C) Several shells are removed between the contacts to gain access to a selected inner shell. (D) A plate and two stator electrodes are fabricated. The structures consist of 10 nm Cr and 25 nm Au. (E) Etching step with BHF.

dispersed onto a 1000 nm oxidized Si wafer from a dispersion in dichloroethane. Thick MWNTs of diameter between 15 and 25 nm are selected with AFM because they are mechanically more robust. The nanotubes are then connected with two electrodes using electron beam lithography (Figure 1B). These electrodes will be used both as conducting electrodes and as anchor pads that hold the nanotube bearing.

In Figure 1C, the electrical-breakdown technique[15−17] is used to remove several outer shells between the electrodes in order to have access to the inner shells. These shells are selectively evaporated stepwise by injecting a large current in the MWNT. The number of removed shells is more than one, typically 5−10, in order to obtain a sliding motion with a lower friction. Indeed, the sliding will occur through a self-selection process between the shells with the most perfect surfaces that offer the least resistance to motion. However, we cannot repeat this process until we are left with one or a very few shells, as the structure is not robust enough to sustain the drying step at the end of the process.

Figure 1D shows the structures that are fabricated in a second lithography step. A 500 nm long plate is attached above the rotating inner shells. The plate is asymmetrically positioned with respect to the tube so that the longer section can be electrostatically attracted to one of the two stator electrodes that are fabricated during the same fabrication step. These 200 nm wide electrodes are designed to be narrow so that they will be deposited on the substrate in the etching step. In such a geometry, the plate moves like a pendulum between the two stator electrodes. If the two stator electrodes were left at the same height as the nanotube, the motion control would be more difficult. For example, the plate may be blocked when it is directed toward one electrode, since voltage application on the other electrode leads to zero electrostatic torque.

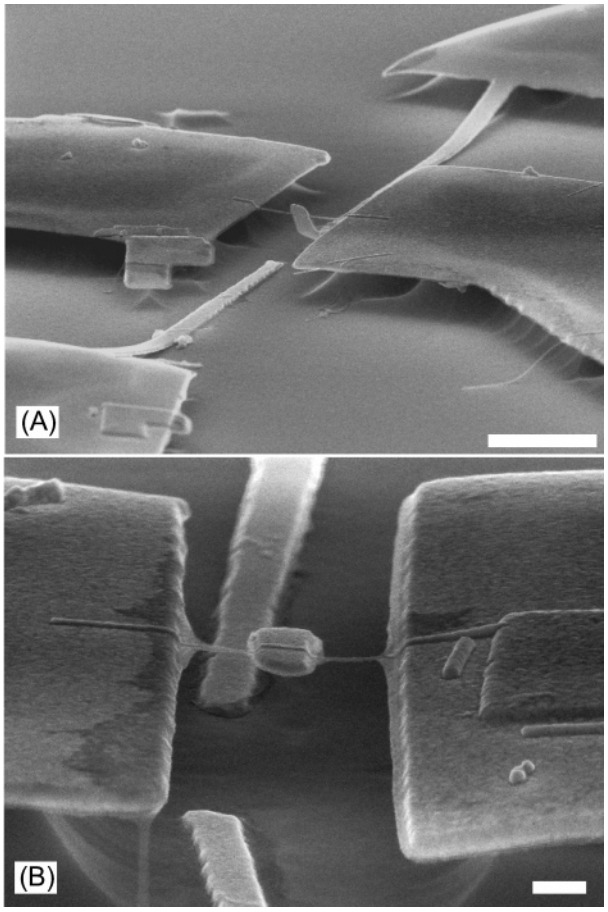

Figure 2. SEM images of two samples at the end of the fabrication process. (A) Scale bar, 1 μm. (b) Scale bar, 200 nm.

The last step of the process consists of etching 500 nm of the SiO_2 with BHF.[18] The wafer is rinsed in DI water and in ethanol. It is then dried under nitrogen flow. The ethanol is heated just below the boiling point in order to reduce surface tension. This reduces the risk of breaking down the structures during drying.

Figure 2 shows two examples of structures obtained at the end of the fabrication process. Interestingly, the plate is not horizontal but has already rotated. The motion has been induced by surface-tension forces of ethanol when drying the sample. Such forces are known to be important and to deform suspended structures in NEMS fabrication. In contrast, it has been shown that the plate stays horizontal for samples where outer shells of the MWNT are not removed.[19] Note that the rotation was observed on most but not all of the samples. In the cases when the plate did not move, some lithography-resist was observed between the plate and the rest of the structure that may have blocked the motion.

We now show that the plate can be electrostatically driven by stator electrodes. Figure 3 shows top down images of the device, made with a scanning electron microscope (SEM) that has been modified in order to electrically access the different electrodes. In Figure 3A the plate is oriented toward the left side stator electrode. To rotate the plate to the right, a bias voltage V is applied between the plate and the right

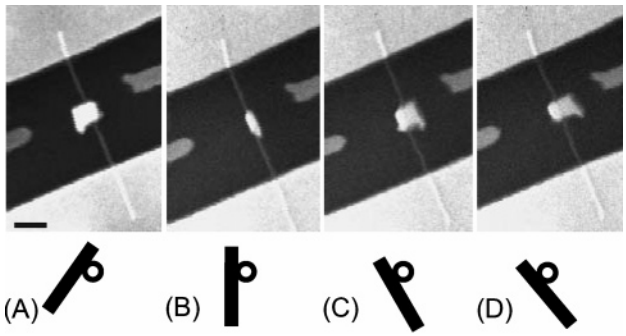

Figure 3. SEM images recorded when (A) $V = 0$ V, $\theta = 0$; (B) $V = 40$ V, $\theta = 35$; (C) $V = 49$ V, $\theta = 65$; (D) $V = 59$ V, $\theta = 75$. The cross-section schematics below each SEM image represent the rotation of the plate around the MWNT. The scale bar is 400 nm.

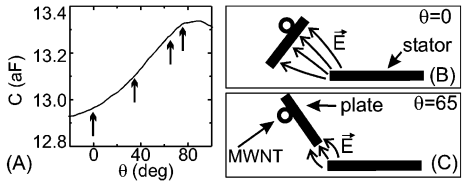

Figure 4. (A) Calculated capacitance between the rotatable plate and the stator electrode as a function of θ. The arrows correspond to the different SEM images. (B) and (C) Electric fields for two different geometries.

side stator electrode. The motion does not happen at once but occurs in the following manner. The voltage is continuously increased from zero while the left side stator electrode and the anchor pads are grounded. The plate stays immobile until 40 V, at which point the plate rotates suddenly to an almost vertical position (Figure 3B). Another angular displacement is observed at 49 V (Figure 3C). The bias has to be increased to 59 V to reach the final position, where the plate faces the biased electrode (Figure 3D).

Importantly, the plate stays in this direction when the bias is turned off. This shows that the rotation is not enabled through the torsion of the tube which would return the plate to the initial position and which occurs for non-engineered MWNTs.[19] We note that the plate stays fixed in this direction even if the maximum V of our source ($V_{max} = 100$ V) is applied on the left side electrode. This electrode lies further away from the tube so that the associated electrostatic torque may not be large enough to initiate the rotation. Indeed, calculations discussed below predict that for motion to be initiated in this geometry, one must apply a voltage $V > V_{max}$. Optimization of the design geometry should solve this.

We now estimate the static friction force. Figure 4A shows calculations using a finite element method program of the capacitance between two plates as a function of angle θ. The two plates describe the rotating plate and the stator electrode, with $\theta = 0$ corresponding to the geometry in Figure 3A. Other elements such as the MWNT or the anchor pads have not been taken into account in the calculations due to the limited capacities of the program. Such elements may screen the electric field and may thus reduce the calculated capacitance value. For example in Figure 4B, the electric field lines go toward the whole plate surface, and part of them may be screened by the nearby MWNT. The situation is different for Figure 4C since the MWNT and the anchor pads lie far away from the electric field lines. This suggests that the capacitance between the rotating plate and the stator electrode is the best described by the calculations when $\theta = 65$ degrees. The friction couple M_{fr} is obtained using $M_{fr} = M_{el} = 0.5\,(dC/d\theta)V^2$ (θ in rad) with the electrostatic couple M_{el} and $V = 59$ V, for which $\theta = 65$ degrees. We estimate then the static friction force $F_{friction} = M_{fr}/r = 48(\pm 5)$ nN, considering that the lever arm r is equal to the radius of the surface where the sliding occurs. Note that r is not known precisely, since sliding occurs through a self-selection process between the shells with the most perfect surfaces. We choose $r = 9(\pm 1)$ nm since it is the mean value of $r = 10$ nm for the pristine MWNT and $r = 8$ nm for the shell on which is attached the rotor.

We assume now that friction is proportional to the contact area. The contact surface is cylindrical, with 1 μm in length and $9(\pm 1)$ nm in radius, which gives a static friction of $0.85(\pm 0.15)$ MPa. This value is close to 0.25−0.75 MPa, the friction measured for high quality crystalline graphite.[20] However, friction in defect-free nanotubes is expected to be lower, since most of the neighbor shells in a MWNT are not commensurate, in contrast with graphite, and since the energetic barrier to intershell sliding has been predicted to be lower for incommensurate shells.[10,11] Moreover, the friction force per surface that we measure is larger than $F_{friction} \sim 0.2$ MPa[8] and $F_{friction} < 0.7$ MPa[7] obtained from measurements of intershell sliding along the nanotube axis. Probably, the enhancement of the friction in our system is related to some disorder centers. The presence of disorder would also explain that the plate is blocked at some specific angles during motion. Further investigation is needed to determine the nature of this disorder, but it might be related to some damage caused by the large current used with the electrical breakdown technique. Note, however, that disorder only weakly increases the intershell friction, leaving possible the activation of the plate motion. This is remarkable given the detrimental effects of sticking in NEMS.

In conclusion, we have developed a fabrication process suitable for the realization of electromechanical rotational actuators. Further work is needed to incorporate a third stator electrode, enabling a complete rotation of the rotating plate. This can be done by fabricating a suspended electrode above the plate. To finish we discuss possible applications of our nanotube-based NEMS. So far, applications of microfabricated motors have not been commercialized. The principal hurdle remains to mechanically transmit the rotation. Our device geometry allows for a simple solution to this. The plate is attached to an inner shell, which is a rotating axle extended over the complete tube. Thus, a long tube can be engineered outside the portion between the two anchor pads. A second plate or a long molecule can then be attached to the rotating inner shells. Note that the device design in ref 4 is different. The rotor plate is attached to the outer shell turning on a much shorter section, which is difficult to exploit.

Acknowledgment. We thank B. Placais, J.M. Berroir, C. Baroud, D. Esteve, P. Joyez, H. Camon, N. Fabre, C. Delalande, and P. Morfin. LPMC is CNRS-UMR8551 associated to Paris 6 and 7. The research in Paris has been supported by the DGA and ACN programs. The work in Lausanne was financed by the Swiss National Science Foundation and its NCCR "Nanoscale Science".

References

(1) *Micromechanics and MEMS: Classic and Seminal Papers to 1990*; Trimmer, W., Ed.; IEEE Press: New York, 1997.
(2) Fan, L. S.; Tai, Y. C.; Muller, R. S. *Proc. 1988 IEEE Int. Electron Devices Meeting;* IEEE Electron Devices Society: San Fransisco, 1988; p 666. Reprinted in ref 1.
(3) Mehregany, M.; Senturia, S. D.; Lang, J. H.; Nagarkar, P. *IEEE Trans. Electron Dev.* **1992**, *39*, 2060.
(4) Fennimore, A. M.; Yuzvinsky, T. D.; Han, W. Q.; Fuhrer, M. S.; Cumings, J.; Zettl, A. *Nature* **2003**, *424*, 408.
(5) Roukes, M. *Phys. World* **2001**, *14*, 57.
(6) Craighead, H. G. *Science* **2000**, *290*, 1532.
(7) Cumings, J.; Zettl, A. *Science* **2000**, *289*, 602.
(8) Yu, M. F.; Yakobson, B. I.; Ruoff, R. S. *J. Phys. Chem. B* **2000**, *104*, 8764.
(9) Charlier, J. C.; Michenaud, J. P. *Phys. Rev. Lett.* **1993**, *70*, 1858.
(10) Kolmogorov, A. N.; Crespi, V. H. *Phys. Rev. Lett.* **2000**, *85*, 4727.
(11) Saito, R.; Matsuo, R.; Kimura, T.; Dresselhaus, G.; Dresselhaus, M. S. *Chem. Phys. Lett.* **2001**, *348*, 187.
(12) Zhao, Y.; Ma, C. C.; Chen, G.; Jiang, Q. *Phys. Rev. Lett.* **2003**, *91*, 175504.
(13) Servantie, J.; Gaspard, P. *Phys. Rev. Lett.* **2003**, *91*, 185503.
(14) Legoas, S. B.; Coluci, V. R.; Braga, S. F.; Coura, P. Z.; Dantas, S. O.; Galvao, D. S. *Phys. Rev. Lett.* **2003**, *90*, 55504.
(15) Collins, P. G.; Arnold, M. S.; Avouris, Ph. *Science* **2001**, *292*, 706.
(16) Collins, P. G.; Hersam, M.; Arnold, M.; Martel, R.; Avouris, Ph. *Phys. Rev. Lett.* **2001**, *86*, 3128.
(17) Bourlon, B.; Glattli, D. C.; Plaçais, B.; Berroir, J. M.; Forró, L.; Bachtold, A. *Phys. Rev. Lett.* **2004**, *92*, 026804.
(18) Nygard, J.; Cobden, D. H. *Appl. Phys. Lett.* **2001**, *79*, 4216.
(19) Williams, P. A.; Papadakis, S. J.; Patel, A. M.; Falvo, M. R.; Washburn, S.; Superfine, R. *Phys. Rev. Lett.* **2002**, *89*, 255502.
(20) Soule, D. E.; Nezbeda, C. W. *J. Appl. Phys.* **1968**, *39*, 5122.

NL035217G